ELSEVIER

Thin Solid Films 322 (1998) 225–232

thin solid films

# A simple indentation stress–strain relation for contacts with spheres on bilayer structures

Xiao Zhi Hu [a,*], Brian R. Lawn [b]

[a] *Department of Mechanical and Materials Engineering, University of Western Australia, Nedlands, WA 6907, Australia*
[b] *Materials Science and Engineering Laboratory National Institute of Standards and Technology, Gaithersburg, MD 20899, USA*

Received 14 August 1997; accepted 30 October 1997

**Abstract**

A simple formulation for the indentation stress–strain behavior of bilayers in contacts with hard spheres is proposed. The formulation is based on empirical power-law stress–strain relations for each of the individual constituent bulk materials, and thence for the bilayer coating/substrate composite. For the constituent materials, two regions of response are considered: at low loads, an elastic region, with linear stress–strain response (exponent = 1); at high loads, an elastic–plastic region, with nonlinear stress–strain response (exponent < 1). The material responses in each of these two regions are characterized by effective moduli. For the composite bilayer, the transition in load-bearing capacity from coating to substrate with increasing load is represented by a three-parameter Weibull asymptotic function of ratio contact radius to coating thickness. This function conveniently defines the geometrical aspects of the contact response separately from the material properties. The power-law formulation is tested, and the Weibull parameters calibrated, against FEM-generated and experimental indentation stress–strain data for selected coating/substrate systems with widely different interlayer elastic–plastic mismatch. The formulation allows a priori predictions of the composite bilayer indentation stress–strain curves from control data on the constituent materials. Conversely, measurements of indentation stress–strain responses on given bilayers may be used to evaluate otherwise undeterminable elastic–plastic properties of coatings on well-characterized substrates. 

*Keywords:* Stress–strain relation; Spheres; Bilayer structures

## 1. Introduction

The relationship between contact load ($P$) and characteristic contact radius ($a$) (or, alternatively, contact displacement ($z$)) represents an important material characteristic in indentations with spheres of given radius ($r$). Spherical indenters are widely studied experimentally, because of their relatively simple geometry; and theoretically, because of their facility to provide essential information on both elastic and plastic deformation properties of the test material [1]. By defining an indentation stress, $p_0 = P/\pi a^2$, and indentation strain, $a/r$, it is possible to generate an indentation function $p_0(a/r)$ which strikingly reflects the intrinsic stress–strain curve for any bulk material. Such functions have been routinely measured on homogeneous bulk materials, including ceramics [1–8].

The problem becomes considerably more complex in the indentation of bilayers, where the contact field can be strongly influenced by elastic–plastic mismatch between the 'coating' and 'substrate' materials. Recently, experimental measurements of indentation stress–strain curves using spherical indenters have been made on a wide variety of coating/substrate systems [9–16]. The complexities are especially severe when the mismatch in material response is large, especially in hard brittle (e.g., ceramic) coatings on soft plastic (e.g., metal, polymer) substrates (or vice versa). In such instances the stress–strain response undergoes a progressive transition, from coating-controlled at very low loads to substrate-controlled at very high loads. Detailed computations using finite element modelling (FEM) codes are able to account for such transitions [14,17]. However, the practical importance of bilayer systems makes it desirable to establish some means of representing the composite stress–strain relation in simple (if empirical) closed form, so that the prospective behavior of any given bilayer structure may be predicted from the properties of the two constituent materials without resort to lengthy numerical computation.

* Corresponding author.

Accordingly, our objective is to formulate a simple $p_0(a/r)$ relation for bilayer composites so that the role of coating thickness and elastic–plastic mismatch as design parameters may be evaluated. We propose power-law relations for $p_0(a/r)$, starting with the separate bulk coating and substrate materials and leading to an analogous power-law expression for the composite bilayers. The relations for the individual materials are linked via an asymptotic function representing the transition in load-bearing capacity from coating to substrate, somewhat analogous to a functional methodology described by Gao et al. [18]. The bilayer relations are tested against FEM-generated and experimental indentation stress–strain data for selected bilayer systems with varying coating thicknesses and widely different interlayer elastic–plastic mismatch. Potential use of the formulation to deconvolute properties of otherwise uncharacterized coatings from indentation measurements on the composite bilayers is discussed.

## 2. Indentation stress–strain curves for bulk materials

The indentation stress–strain relation $p_0(a/r)$ for contacts with spheres is well defined by the classic Hertzian theory for ideally elastic, homogeneous bulk materials of Young's modulus $E$ and Poisson's ratio $\nu$ [19,20]. The Hertzian solution for $p_0(a/r)$ has the linear form [2]

$$p_0 = (4E'/3\pi)(a/r) \tag{1}$$

where we define a modified Young's modulus for the indenter/specimen system,

$$E' = 1/\left[(1-\nu^2)/E + \left(1-\nu_I^2\right)/E_I\right] \tag{2}$$

with I referring to the indenter material. The indentation stress–strain curve in Eq. (1) reflects the elastic stress–strain response of the test material, and its uniqueness is unaffected by the size of the indenting sphere.

Experimental data on monolithic materials confirm that $p_0(a/r)$ is independent of sphere size even when plastic damage occurs below the contact ('geometrical similarity' [1]). To exploit the general usefulness of this result, Eq. (1) needs to be extended to cover nonlinearity. We propose the following simple modification:

$$p_0 = (4E^*/3\pi)(a/r)^n \tag{3}$$

with material parameters $E^*$ a nonlinear modulus and $n$ a strain-hardening parameter. Eq. (1) is recovered if $n=1$ and $E^* = E'$. The parameters $n\,(\le 1)$ and $E^*\,(\le E')$ may be obtained by curve-fitting numerically (e.g., FEM) generated or direct experimental data on any given inelastic monolithic material.

Generally, it is necessary to assign different values of $n$ and $E^*$ in different regions of the stress–strain curve, to distinguish low-load elastic responses (Eq. (1)) from high-load plastic responses (Eq. (3)) in materials with distinctive elastic–plastic regions [21].

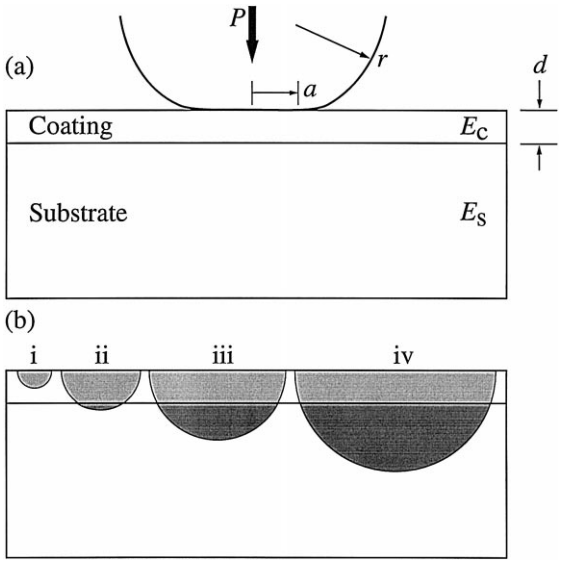


Fig. 1. Contact of a sphere on a coating/substrate bilayer system. (a) Showing key indentation variables. (b) Showing expansion of idealized deformation zone with increasing load, $i \rightarrow ii \rightarrow iii \rightarrow iv$. Load sequence represents transition from coating-controlled response in $i$ to substrate-controlled response in $iv$. In real bilayers with large elastic–plastic mismatch the deformation zone may depart significantly from the hemispherical configuration depicted here.

## 3. Indentation stress–strain curves for composite bilayers

Consider the contact of a bilayer system with a sphere, as depicted in Fig. 1a. The volumes of influence of the deformation field are idealized by hemispherical zones about the contact center. Two factors distinguish the bilayer from the bulk structure: (i) a configurational factor $d/r$, representing the coating thickness $d$ in relation to the sphere radius $r$; (ii) a material factor $E_c/E_s$ ($E_c'/E_s'$ or $E_c^*/E_s^*$) representing the coating/substrate elastic–plastic mismatch. It can be foreseen from the idealized deformation geometry in Fig. 1b that the substrate will have little influence on the $p_0(a/r)$ relation when the contacts are small, $a/d \ll 1$; conversely, the substrate will exert a strong, even dominant influence when the contacts are large, $a/d \gg 1$. The critical questions are: can we define a universal configurational function to describe the transition between these two limiting cases?—and how does the mismatch term $E_c/E_s$ enter into this function? Of course, in real bilayers the deformation geometry may depart substantially from the idealized configuration shown in Fig. 1, with enhanced damage zone in either the coating or substrate depending on the mismatch, in which case the

universality of any derived configurational function is questionable. However, as we shall see, a reasonably well-defined function can be determined for a broad range of material bilayers.

As in the previous section, we begin by first considering elastic contacts (cf. Eq. (1)), and then generalizing the treatment to plastic contacts (cf. Eq. (3)).

### 3.1. Fully elastic response

Begin by considering relations for the contact radius $a$ and load $P$ in terms of the effective elastic modulus $E'$ for the constituent bulk coating (c) and substrate (s) materials. From Eq. (1), in conjunction with $p_0 = P/\pi a^2$:

$$a_c = (3Pr/4E'_c)^{1/3} \tag{4a}$$

$$a_s = (3Pr/4E'_s)^{1/3} \tag{4b}$$

Suppose that we write an analogous relation for the composite coating/substrate bilayer (cs):

$$a = (3Pr/4E'_{cs})^{1/3} \tag{5}$$

with $E'_{cs}$ an effective modulus for the bilayer. We can expect Eq. (5) to approach Eq. (4a) asymptotically at $a/d \ll 1$ (low $P$), and conversely Eq. (4b) asymptotically at $a/d \gg 1$ (high $P$), as indicated schematically in Fig. 2. In the intermediate region, $E'_{cs}$ will depend on the mismatch parameter $E'_c/E'_s$ and configuration variable $a/d$.

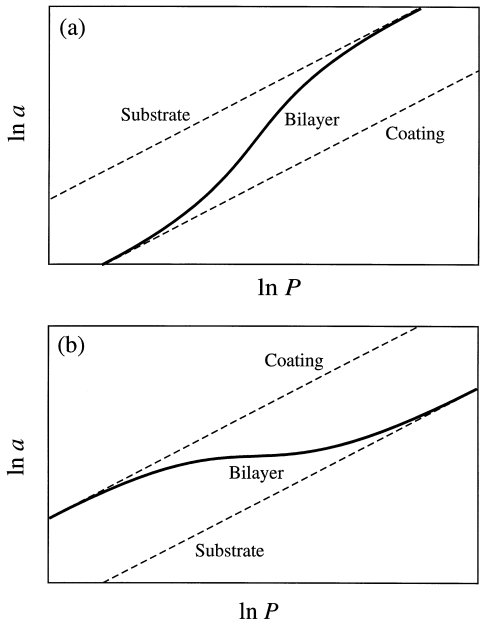


Fig. 2. Asymptotic behavior of $a(P)$ in Eq. (5) for bilayer, depicted schematically for (a) hard coating on soft substrate, (b) soft coating on hard substrate. Dashed lines are representations of Eqs. (4a) and (4b) for the monolithic coating and substrate materials respectively.

In order to evaluate $E'_{cs}$ we adopt a procedure analogous in some ways to that used by Gao et al. [18] for elastic contacts on bilayers. We rewrite Eq. (5) in the reduced form

$$a = a_c(E'_c/E'_s)^{L/3} \tag{6}$$

such that, with Eqs. (4a) and (4b), the exponent $L$ defines a nondimensional configurational function

$$L(a/d) = \ln(a/a_c)/\ln(a_s/a_c) \tag{7}$$

with $0 \le L \le 1$ in the region $0 \le a/d \le \infty$. The function $L(a/d)$ bears some resemblance to the modulus weighting function ('fraction coefficient') defined by Gao et al. [18] although the mathematical context in the present work is quite different. Along with $p_0 = P/\pi a^2$, Eq. (6) provides the indentation stress–strain relation for elastic bilayers:

$$p_0 = (4E'_c/3\pi)(E'_s/E'_c)^L(a/r) \tag{8}$$

In this relation the influence of the substrate is seen as a simple modification of the elastic response for the bulk coating, with mismatch factor $E'_c/E'_s$ and configuration factor $L(a/d)$ now conveniently separated. This separation is helpful because it allows us to study the mismatch and geometry factors independently. From Eqs. (4a), (4b), (5) and (6), the effective modulus for the bilayer is

$$E'_{cs}(a/d) = E'_c(E'_s/E'_c)^{L(a/d)} \tag{9}$$

Note that in the trivial case of zero mismatch in Eq. (9) ($E'_{cs} = E'_c = E'_s$), Eq. (8) reduces to Eq. (1) for the bulk coating ($L = 0$, $a/d = 0$) or substrate ($L = 1$, $a/d = \infty$).

This leaves only determination of the configurational asymptotic function $L(a/d)$. We shall return to this issue in Section 4, after extending the analysis to elastic–plastic contacts.

### 3.2. Elastic–plastic response

The analysis for elastic bilayers may be extended to cover elastic–plastic bilayers by replacing Eq. (1) with Eq. (3). We write separate indentation stress–strain relations for coating (c) and substrate (s):

$$p_{0c} = (4E^*_c/3\pi)(a_c/r)^n \tag{10a}$$

$$p_{0s} = (4E^*_s/3\pi)(a_s/r)^m \tag{10b}$$

where $n$ and $m$ are plasticity exponents and $E^*_c$ and $E^*_s$ are effective nonlinear moduli. With $p_0 = P/\pi a^2$, we obtain analogous expressions for the contact radii $a$ in Eqs. (4a) and (4b):

$$a_c = (3Pr^n/4E^*_c)^{1/(n+2)} \tag{11a}$$

$$a_s = (3Pr^m/4E^*_s)^{1/(m+2)} \tag{11b}$$

Following Eq. (5), we write an analogous relation for the coating/substrate (cs) bilayer:

$$a = \left(3Pr^N/4E_{cs}^*\right)^{1/(N+2)} \tag{12}$$

where $E_{cs}^*$ is an effective modulus and $N$ is an effective exponent in the elastic–plastic region.

Presuming the function $L(a/d)$ in Eq. (7) to remain material-insensitive, the analysis yields a nonlinear stress–strain relation for bilayers:

$$p_0 = \left(4E_c^*/3\pi\right)\left(E_s^*/E_c^*\right)^l (a/r)^{n-(n-m)l} \tag{13}$$

where $l$ is another nondimensional configurational exponent,

$$l(a/d) = (n+2)L(a/d)/\left[(m+2) + (n-m)L(a/d)\right] \tag{14}$$

Like $L(a/d)$, $l(a/d)$ is an asymptotic function, with similar limits, i.e., $l=0$ at $L=0$ $(a/d=0)$ and $l=1$ at $L=1$ $(a/d=\infty)$. Within these limits, $l>L$ $(0\le a/d\le\infty)$. Again, the influence of the substrate represents a simple modification of the elastic–plastic response for the bulk coating, with mismatch factor $E_s^*/E_c^*$ and configuration factor $l(a/d)$ separate entities. From Eqs. (12) and (13), the effective modulus and exponent are determined as

$$E_{cs}^*(a/d) = E_c^*\left(E_s^*/E_c^*\right)^{l(a/d)} \tag{15a}$$

$$N(a/d) = n - (n-m)l(a/d) \tag{15b}$$

Note that in the trivial case of zero mismatch ($E_{cs}^* = E_c^* = E_s^*$; $N=n=m$), we have $l=L$ in Eq. (14), in which case Eq. (13) reduces to Eq. (3) for the bulk coating ($L=0$, $a/d=0$) or substrate ($L=1$, $a/d=\infty$).

Again, the stress–strain curve is asymptotically determined by the properties of the coating at small contacts ($a/d\to 0$), and by the properties of the substrate at large contacts ($a/d\to\infty$). For the special case of identical exponents $m=n$ ($l=L$ in Eq. (14)), Eq. (13) reduces to

$$p_0 = \left(4E_c^*/3\pi\right)\left(E_s^*/E_c^*\right)^L (a/r)^n \tag{16}$$

For the even more special case $m=n=1$, the elastic solution of Eq. (8) is recovered.

## 4. Empirical calibration of asymptotic configuration functions

We are now left with determining the asymptotic configuration function $L(a/d)$, and thence $l(a/d)$, needed for predicting the response of the bilayer from the elastic–plastic constants of the individual coating and substrate materials. We resort here to empirical calibration, using $p_0(a/r)$ data for selected bilayer systems with a wide range of elastic–plastic mismatch: (i) a relatively hard glass–ceramic coating (Dicor, Dentsply/Caulk, Milford, DE) on a soft glass-filled polymer substrate (HCE, Kuraray, Osaka, Japan) [22]; (ii) a relatively soft porcelain coating (Vita ZahnFabrik, Bad Sackingen, Germany) on a hard glass-infiltrated alumina substrate (InCeram, Vita ZahnFabrik, Bad Sackingen, Germany) [22]; (iii) a hard silicon nitride coating on a softened silicon nitride containing 30 vol.% boron nitride platelets ($Si_3N_4/Si_3N_4$–30BN) [16,23]. Data for the first two systems are computer-generated in stepwise loading using an FEM algorithm for Hertzian contacts on layer structures, in conjunction with constitutive relations matching the elastic–plastic properties of the individual bulk materials [14] (Appendix A). Data for the silicon nitride system are taken from actual

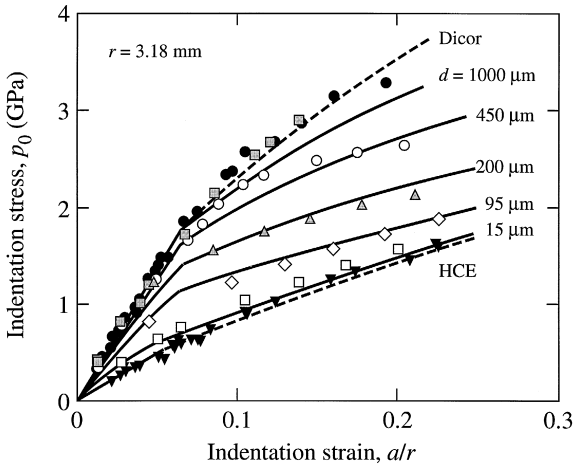


Fig. 3. Indentation stress–strain curve for Dicor glass–ceramic coatings on HCE polymer substrates, for coating thicknesses $d$ indicated. Data points are FEM-generated results, using WC spheres $r=3.18$ mm for bilayer data. Solid curves are generated from Eqs. (8), (10a) and (10b). Bounding curves for Dicor and HCE bulk materials are data fits; intermediate curves for bilayer data at prescribed coating thickness $d$ are predictions. (Data courtesy of I.M. Peterson, Y.-G. Jung and S. Wuttiphan.)

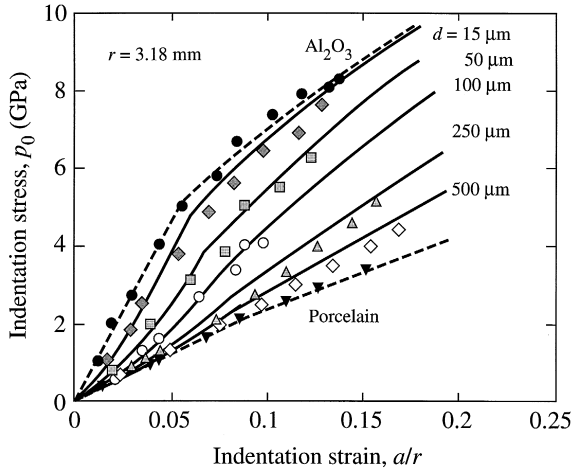


Fig. 4. Indentation stress–strain curve for porcelain coatings on glass-infiltrated alumina substrates, for coating thicknesses $d$ indicated. Data points are FEM-generated results, using WC spheres $r=3.18$ mm for bilayer data. Solid curves are generated from Eqs. (8), (10a) and (10b). Bounding curves for porcelain and alumina bulk materials are data fits; intermediate curves for bilayer data at prescribed coating thickness $d$ are predictions. (Data courtesy of I.M. Peterson and S. Wuttiphan.)

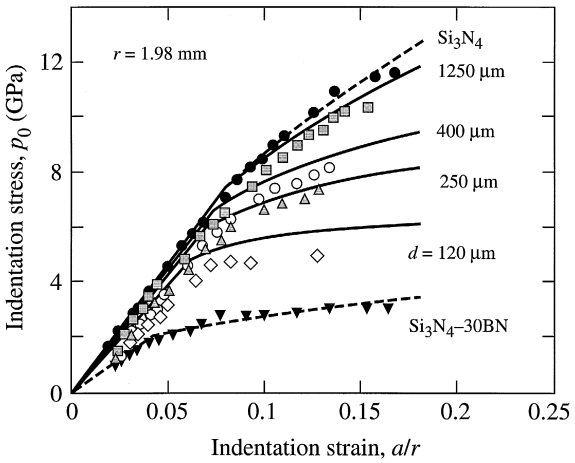


Fig. 5. Indentation stress–strain curves for $Si_3N_4$ coatings on $Si_3N_4$–30 wt.% BN substrates, for coating thicknesses $d$ indicated. Data points are experimental results, using WC spheres $r = 1.98$ mm for bilayer data. Solid curves are generated from Eqs. (8) and (13), in conjunction with Eqs. (14) and (17). Bounding curves for $Si_3N_4$ and $Si_3N_4$–30 wt.% BN bulk materials are data fits; intermediate curves for bilayer data at prescribed coating thickness $d$ are predictions. (Data from Ref. [16].)

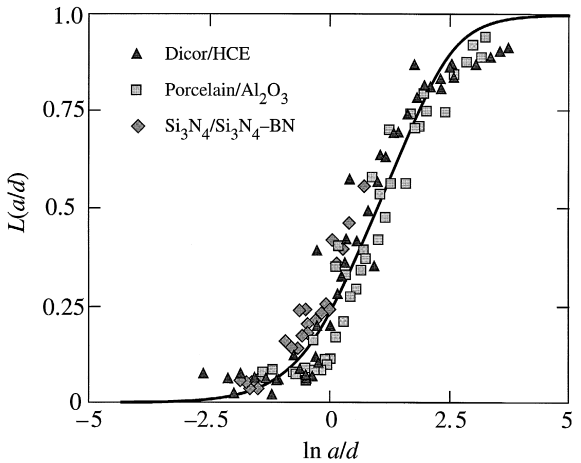


Fig. 6. Determination of configuration function $L(a/d)$. Points are from bilayer data in Figs. 3, 4 and 5. Solid curve is best-fit three-parameter Weibull function.

experimental measurements of contact radii over a range of contact loads [16]. In practice, the coatings in each of these material systems may be subject to some transverse (and perhaps also delamination) cracking at high loads [16,22,23], limiting the capacity to match experimental data in the upper regions of the stress–strain curve.

The indentation stress–strain data for the three bilayer systems are plotted in Figs. 3–5, for a range of coating thicknesses $d$, and for tungsten carbide spheres of radius $r = 3.18$ mm in Figs. 3 and 4 and $r = 1.98$ mm in Fig. 5. Data for the constituent bulk materials represent upper and lower bounds for the bilayer functions. Best fits of Eqs. (1) and (3) to these bounding data in the elastic and elastic–plastic regions are shown as dashed curves. We distinguish the elastic and plastic regions arbitrarily by $a/r = 0.05$, corresponding to a typical indentation strain at yield [1]. (Alternatively, and perhaps preferably, one might distinguish the two regions by actual measurements of the contact pressure $p_Y$ at which yield is first observed experimentally [1,24–26].) The best fits to the bulk material data enable the evaluations of the coating and substrate moduli ($E_c'$ and $E_s'$, $E_s^*$ and $E_c^*$) and exponents ($n$ and $m$) in Table 1.

With this parametric calibration for the constituent materials, we then use the bilayer data in Figs. 3–5 to determine $L$ as a function of $a/d = (a/r)(r/d)$, solving from Eq. (8) (elastic) or Eqs. (13) and (14) (elastic–plastic). The results for the three bilayer systems are plotted in Fig. 6. Note that the $L(a/d)$ data for the three systems overlap each other within the random scatter in data, suggesting a universal function, although some systematic shifts are apparent. The data are best-fitted by a three-parameter Weibull function,

$$L(a/d) = 1 - \exp\left\{-\left[A + B\ln(a/d)\right]^M\right\} \qquad (17)$$

yielding coefficients $A = 0.749$, $B = 0.173$ and $M = 4.72$. This best-fit function is plotted as the solid curve in Fig. 6. Note that the data tend asymptotically to the limits $L = 0$ at $a/d = 0$ and $L = 1$ at $a/d = \infty$, as required.

To illustrate the validity of this fitting procedure, we regenerate the indentation stress–strain functions $p_0(a/r)$ from Eqs. (8) and (13) for the bilayers as the solid curves in Figs. 3–5, using the best-fit function $L(a/d)$ in Eq. (17) together with the empirically calibrated material parameters in Table 1. Notwithstanding some systematic deviations from the data, the regenerated curves account for the broad trend from coating-controlled to substrate-controlled behavior as the indentation strain $a/r$ increases, and as the coating thickness $d$ diminishes.

Table 1
Elastic–plastic parameters in Eq. (1) for bulk coating (c) and substrate (s) materials represented in Figs. 3, 4 and 5

| Material | | Elastic modulus (GPa) | Inelastic modulus (GPa) | Inelastic exponent |
|---|---|---|---|---|
| Glass–ceramic (Dicor) | (c) | $E_c = 64.1$ | $E_c^* = 22.4$ | $n = 0.614$ |
| Polymer (HCE) | (s) | $E_s = 23.5$ | $E_s^* = 11.5$ | $m = 0.764$ |
| Porcelain | (c) | $E_c = 54.8$ | $E_c^* = 39.7$ | $n = 0.852$ |
| $Al_2O_3$ (infiltrated) | (s) | $E_s = 218$ | $E_s^* = 57.6$ | $m = 0.540$ |
| $Si_3N_4$ | (c) | $E_c = 220$ | $E_c^* = 89.0$ | $n = 0.639$ |
| $Si_3N_4$–30BN | (s) | $E_s = 113$ | $E_s^* = 15.0$ | $m = 0.368$ |

## 5. Discussion

In this study we have presented simple, analytical power-law relations for the stress–strain response $p_0(a/r)$ of elastic–plastic bilayer systems (Sections 2 and 3) for indentations with spheres. The configurational function $L(a/d)$ that lies at the core of the analysis has been evaluated from data on three material bilayer systems, and fitted with an empirical three-parameter Weibull function (Section 4). A feature of the formulation is the mathematical separation of material parameters (mismatch modulus factors $E_c'/E_s'$ and $E_c^*/E_s^*$, exponents $n$ and $m$) from geometrical parameters ($a/d$, or $d/r$), so that the roles of material and geometrical variables may be assessed independently. To make predictions for a given bilayer system it is still necessary to specify material parameters a prior for each layer component, or to calibrate these parameters directly from experimentally measured or FEM-generated data on monolith controls. The ensuing calculation of the composite $p_0(a/r)$ function using Eqs. (8) and (13) is more straightforward than conventional numerical analysis. In this context, the power-law formulation presents itself as a useful design adjunct for optimizing materials and geometries for layer structures.

The fact that we can fit a single function to the data in Fig. 6 for widely different coating/substrate bilayer systems suggests a certain universality in our function $L(a/d)$ for spherical indenters, providing confidence in using the analysis in a predictive capacity. Universality in $L(a/d)$ implies geometrical similarity in the contact field, essentially requiring that the geometry of the damage zones in Fig. 1b be the same for all material systems. This requirement is in fact unlikely to be satisfied for materials with widely different modulus and hardness properties, especially in the elastic–plastic regions where yield occurs preferentially and more extensively in the softer component [16,23]. Such departures from similarity could account for the small apparent system-to-system data shifts in Fig. 6, and thence for some of the discrepancies between data and predictions in Figs. 3–5. Nevertheless, the predicted curves do appear to predict the broader data trends in these figures.

In principal, one could derive analogous $L(a/d)$ functions for contacts with fixed-profile indenters, e.g., cones or pyramids, in terms of the (size-invariant) hardness values of the coating and substrate materials [17]. The advantage of spherical indenters is that they incorporate the complete range of elastic and plastic properties within the constituent $p_0(a/r)$ functions [21,25,27], whereas the same functions for fixed-profile indenters (at least in the loading half-cycle of the indentation) contain information only on the fully plastic state.

In the present work we have chosen bilayers with coating thicknesses in the range $\approx 0.1$–1 mm as illustrative case studies. However, universality in $L(a/d)$ means that the analysis should apply equally well to microscale and even nanoscale layers—it is necessary only to scale the indentation process to suit the scale of the coating. To establish a rule of thumb for this scaling we write $r/d = (r/a)(a/d)$, and insert the following representative values: (i) $a/d = 2.77$ at $L = 0.5$ in Eq. (17) (Fig. 6), corresponding to a contact configuration in which the substrate and coating contribute equally to the load-bearing capacity; (ii) $a/r = 0.1$, corresponding to the mid-range of elastic–plastic deformation (Figs. 3–5). This gives $r/d \approx 25$. Hence our use of sphere radius $r = 1.98$ and 3.18 mm is most appropriate to coatings of thickness $d \approx 0.1$ mm. Conversely, for $d = 1$ $\mu$m and $d = 1$ nm, we would choose spheres of radius $r \approx 25$ $\mu$m and $r \approx 25$ nm, respectively, which is in the range of instrumented nanoindenters.

We have used the properties of the constituent bulk materials to predict the indentation stress–strain response of composite bilayers. In many coating systems this course may not always be possible, because of difficulties in obtaining bulk specimens of the coating material for independent evaluation. Moreover, the properties of coatings may be very different from those of the corresponding bulk material. (A striking example is plasma-sprayed coatings, where the moduli may be diminished by more than an order of magnitude [12].) In this context, a potentially important application of our simple formulation is to deconvolute the coating properties from measurements on the composite bilayers. In principle, one should be able to evaluate all of the coating and substrate parameters (moduli $E_c'$ and $E_s'$, $E_s^*$ and $E_c^*$, exponents $n$ and $m$) by best-fitting the bilayer data sets to Eqs. (8) and (13) in the elastic and elastic–plastic regions, in conjunction with Eqs. (14) and (17). In practice, the reliability of any such evaluation will depend on the availability of a sufficient quantity of data; and, in the case of the coating, will be greatly improved if the properties of the substrate are

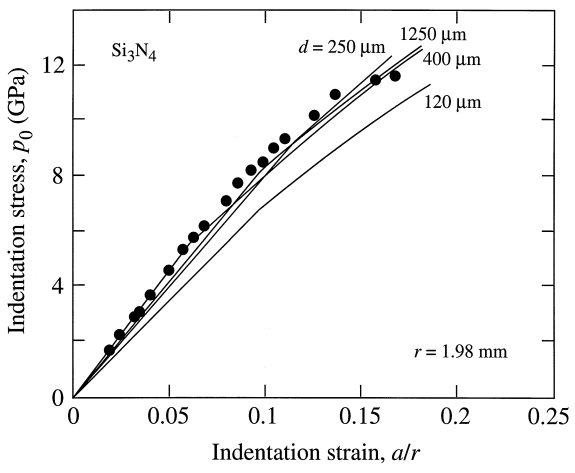


Fig. 7. Plot of indentation stress–strain curves for $Si_3N_4$ coating material. Data points are experimental measurements from Fig. 5. Solid curves are predictions from Eqs. (1) and (3) using coating parameters deconvoluted from bilayer data in Fig. 5.

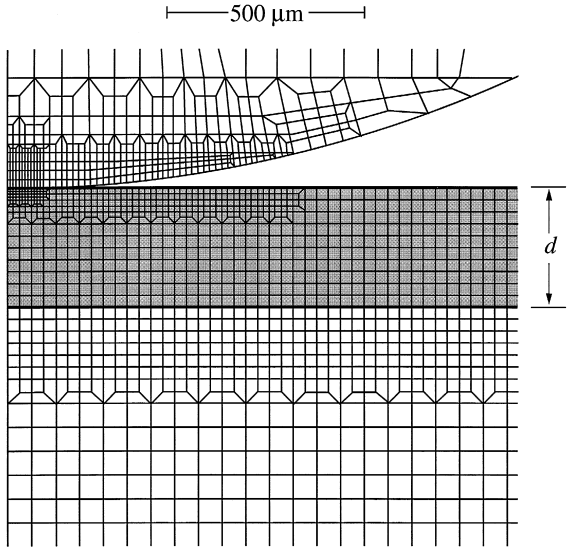


Fig. 8. Finite element grid for indentation of bilayer of coating thickness $d$ with sphere of radius $r$ (3.18 mm).

independently established. As an example, we use the bilayer data sets for each coating thickness $d$ in Fig. 5 to determine the parameters for the silicon nitride coating material, using the substrate parameters listed in Table 1. With these determinations, we regenerate the coating stress–strain functions (solid curves) shown in Fig. 7, for comparison with the experimental data points. The correlation between predicted curves and experimental data is generally well within 10% in stress values, except for the smallest coating thickness $d$. The discrepancy in the latter case confirms that more reliable evaluations of the coating properties are likely to come from data at larger $d$.

Our power-law stress–strain formulation, notwithstanding its apparent capacity to predict trends, has acknowledged limitations. We have already alluded to departures from universal geometrical similarity as one such limitation. Invariably, adoption of empirical power-law functions provides mathematical expediency at the expense of physical insight. Such idealized power-law functions are unlikely to represent fundamental uniaxial stress–strain responses. (In fact, in quasi-plastic materials, the underlying elastic–plastic response is probably closer to bilinear [28], resulting in a nonlinear $p_0(a/r)$ function different from power-law [21].) We may expect the regenerated $p_0(a/r)$ curves to provide inaccurate representations in the transition region near the yield point, and at high stresses and strains as the deformation approaches full plasticity. In brittle coatings on soft substrates, experimental data points are expected to fall below the regenerated curves at high loads, as transverse cracks propagate and reduce the net compliance of the system [13,22]. (However, note that delamination cracks are less likely to influence the results, since these cracks tend to form predominantly at the end of unloading [13].) We may further expect the regenerated curves to be inaccurate in the presence of superposed residual in-plane coating stresses, e.g., from thermal expansion mismatch between interlayers, especially for residual stresses > 1 GPa (cf. values of $p_0$ in Figs. 3–5). FEM simulations are likely to provide more accurate and continuous representations over the data range, especially in the vicinity of the yield point [14,15], and if due allowance is also made in the code for the incidence of any transverse cracking [29].

Finally, it is envisioned that the procedure outlined in Sections 2 and 3 might equally well be used to derive load-displacement ($P$–$z$) relations of the kind measured in instrumented indentation testing [30,31].

## Acknowledgements

Funding from the Australian Research Council and from the US Air Force Office of Scientific Research is acknowledged. The authors are grateful to S. Wuttiphan, I.M. Peterson and Y.G. Jung for providing the FEM data sets in Figs. 3 and 4 and Eq. (A1b), and to K.S. Lee and S.K. Lee for providing the experimental data in Fig. 5.

## Appendix A. Finite element modelling of indentation stress–strain curves

A commercial FEM package (Strand, G&D Computing, Sydney, Australia) is used to construct an algorithm for generating the data in Figs. 3 and 4 [14,15]. The algorithm models an indenting sphere of given radius ($r = 3.18$ mm) in frictionless axisymmetric contact on a flat cylindrical specimen (4 mm radius and 4 mm thick), using the grid shown in Fig. 8. For the bilayer structures, each material layer is allowed to yield according to a

Table 2
Material parameters in constitutive relation Eq. (A1a) for bulk coating and substrate materials represented in Figs. 3 and 4

| Material | Young's modulus [$E$] (GPa) | Yield stress [$Y$] (GPa) | Strain-hardening coefficient [$\alpha$] |
|---|---|---|---|
| Glass–ceramic (Dicor) | 69.0 | 1.95 | 0.40 |
| Polymer (HCE) | 25.0 | 0.59 | 0.75 |
| Porcelain | 66.6 | 1.95 | 1.00 |
| $Al_2O_3$ (infiltrated) | 252 | 4.35 | 0.40 |

critical shear stress condition, in conjunction with a bilinear uniaxial stress–strain function $\sigma(\varepsilon)$ [25]:

$$\sigma = E\varepsilon, \quad (\sigma < Y) \tag{A1a}$$

$$\sigma = Y + \alpha(\varepsilon E - Y), \quad (\sigma > Y) \tag{A1b}$$

with $E$ Young's modulus, $Y$ a uniaxial compression yield stress, and $\alpha$ a dimensionless strain-hardening coefficient ($0 \le \alpha \le 1$: $\alpha = 1$, fully elastic; $\alpha = 0$, fully plastic). Strong interfacial bonding is assumed between the adjacent layers in Fig. 8 (no delamination). Contact is incremented monotonically to peak load, with a maximum 50 iterations at each increment, with a tolerance 0.1% in force and 0.5% in displacement. At each load $P$ the contact radius $a$ is determined, from which $p_0 = P/\pi a^2$ and $a/r$ are evaluated.

In order to generate a priori FEM stress–strain curves for the bilayers of specified coating thicknesses $d$ in Fig. 8, the parameters, $E$, $Y$ and $\alpha$ in Eq. (1) (as well as Poisson's ratio-taken here at a common value 0.25), must first be specified for each material. In practice, this is most readily done by 'calibration' against experimental $p_0(a/r)$ data for bulk specimens. The results of such parameter calibrations for the materials in Figs. 3 and 4 are summarized in Table 2, to be described in more detail elsewhere [22].

## References

[1] D. Tabor, Hardness of Metals, Clarendon, Oxford, 1951.
[2] M.V. Swain, B.R. Lawn, Phys. Status Solidi 35 (1969) 909.
[3] M.V. Swain, J.T. Hagan, J. Phys. D 9 (1976) 2201.
[4] F. Guiberteau, N.P. Padture, H. Cai, B.R. Lawn, Philos. Mag. A 68 (1993) 1003.
[5] H. Cai, M.A. Stevens Kalceff, B.R. Lawn, J. Mater. Res. 9 (1994) 762.
[6] N.P. Padture, B.R. Lawn, J. Am. Ceram. Soc. 77 (1994) 2518.
[7] H.H.K. Xu, L. Wei, N.P. Padture, B.R. Lawn, R.L. Yeckley, J. Mater. Sci. 30 (1995) 869.
[8] A. Pajares, L. Wei, B.R. Lawn, D.B. Marshall, J. Mater. Res. 10 (1995) 2613.
[9] D.F. Diao, K. Kato, K. Hokkirigawa, Trans. ASME J. Tribology 116 (1994) 860.
[10] L. An, H.M. Chan, N.P. Padture, B.R. Lawn, J. Mater. Res. 11 (1996) 204.
[11] S. Wuttiphan, B.R. Lawn, N.P. Padture, J. Am. Ceram. Soc. 79 (1996) 634.
[12] A. Pajares, L. Wei, B.R. Lawn, N.P. Padture, C.C. Berndt, Mater. Sci. Eng. A 208 (1996) 158.
[13] A. Pajares, L. Wei, B.R. Lawn, C.C. Berndt, J. Am. Ceram. Soc. 79 (1996) 1907.
[14] A.C. Fischer-Cripps, B.R. Lawn, A. Pajares, L. Wei, J. Am. Ceram. Soc. 79 (1996) 2619.
[15] S. Wuttiphan, A. Pajares, B.R. Lawn, C.C. Berndt, Thin Solid Films 293 (1997) 251.
[16] K.S. Lee, S. Wuttiphan, X.Z. Hu, S.K. Lee, B.R. Lawn, J. Am. Ceram. Soc. (in press).
[17] A.K. Bhattacharya, W.D. Nix, Int. J. Solids Struct. 24 (1988) 1287.
[18] H. Gao, C.-H. Chiu, J. Lee, Int. J. Solids Struct. 29 (1992) 2471.
[19] H. Hertz, Hertz's Miscellaneous Papers, Macmillan, London, Chaps. 5–6, 1896.
[20] K.L. Johnson, Contact Mechanics, Cambridge Univ. Press, London, 1985.
[21] A.C. Fischer-Cripps, B.R. Lawn, Acta Metall. 44 (1996) 519.
[22] Y.G. Jung, S. Wuttiphan, I.M. Peterson, B.R. Lawn, J. Dent. Res. (in preparation).
[23] H. Liu, B.R. Lawn, S.M. Hsu, J. Am. Ceram. Soc. 79 (1996) 1009.
[24] R.M. Davies, Proc. R. Soc. London A 197 (1949) 416.
[25] A.C. Fischer-Cripps, B.R. Lawn, J. Am. Ceram. Soc. 79 (1996) 2609.
[26] S.K. Lee, S. Wuttiphan, B.R. Lawn, J. Am. Ceram. Soc. 80 (1997) 2367.
[27] A.C. Fischer-Cripps, J. Mater. Sci. 32 (1997) 727.
[28] B.R. Lawn, D.B. Marshall, J. Mech. Phys. Solids 46 (1998) 85.
[29] C. Kocer, R.E. Collins, J. Am. Ceram. Soc. (in press).
[30] M.V. Swain, J. Mencik, Thin Solid Films 253 (1994) 204.
[31] Y. Sun, A. Bloyce, T. Bell, Thin Solid Films 271 (1995) 122.